Remote Sensing of Environment 201 (2017) 1–11

Contents lists available at ScienceDirect

Remote Sensing of Environment

journal homepage: www.elsevier.com/locate/rse

The mSCOPE model: A simple adaptation to the SCOPE model to describe reflectance, fluorescence and photosynthesis of vertically heterogeneous canopies

Peiqi Yang*, Wout Verhoef, Christiaan van der Tol

Faculty of Geo-Information Science and Earth Observation (ITC), University of Twente, P.O. Box 217, Enschede 7500 AE, The Netherlands

ARTICLE INFO

Keywords:
SCOPE
Vertical heterogeneity
Radiative transfer model
Chlorophyll fluorescence
Photosynthesis

ABSTRACT

The vertical heterogeneity of leaf biophysical and biochemical properties may have a large effect on the bi-directional reflectance and fluorescence of vegetation canopies. This has implications for the interpretation of remote sensing data. We developed a model for light interaction and energy balance in vegetation canopies in which leaf biophysical and biochemical properties vary in the vertical. The model mSCOPE is an extension of the Soil-Canopy Observation of Photosynthesis and Energy fluxes (SCOPE) model, which simulates spectral and bidirectional reflectance, fluorescence, and photosynthesis of vertically heterogeneous vegetation canopies. The modelling of radiative transfer in mSCOPE is based on the classical SAIL theory. A solution to the radiative transfer equation for multi-layer canopies is given, which allows calculating top-of-canopy (TOC) reflectance and the flux profile. The latter is used for the simulation of fluorescence emission and photosynthesis of every leaf through the leaf radiative transfer model Fluspect and a biochemical model. The radiative transfer of fluorescence in multi-layer canopies is solved numerically in mSCOPE to obtain TOC bidirectional fluorescence. The significant effect of vertical heterogeneity of leaf properties on TOC reflectance, fluorescence and photosynthesis is demonstrated by different scenarios with customized vertical profiles of leaf chlorophyll content and leaf water content, and also with measured vertical profiles of leaf chlorophyll content in corn canopies. A preliminary validation of the reflectance calculating routine of mSCOPE is conducted by comparing measured and simulated TOC reflectance spectra of the corn canopies. We conclude that it is important to consider the vertical heterogeneity of leaf properties for the prediction of reflectance, fluorescence and photosynthesis. The model mSCOPE could serve as a tool to better understand vertically heterogeneous vegetation canopies.

1. Introduction

Vegetation models are powerful tools to understand a variety of plant physiological processes. Radiative transfer models (RTMs), as a major class of vegetation models, are widely used in remote sensing applications because they offer an explicit connection between the top of canopy (TOC) observations and vegetation properties (e.g., chlorophyll, leaf area index) (Houborg et al., 2007; Ustin et al., 2009). Vegetation models that simulate photosynthesis (De Wit, 1962; Myneni, 1991) include, besides an RTM, also a leaf photosynthesis model such as Farquhar et al. (1980) or Collatz et al. (1992). The RTM simulates the light distribution within the canopy, while the photosynthesis model simulates the energy partitioning in photosystems.

SCOPE (Soil Canopy Observation, Photochemistry and Energy fluxes) is an integrated radiative transfer and energy balance model (Van der Tol et al., 2009) that simulates the spectrum of TOC reflected radiation, fluorescence emission in the viewing direction and photosynthesis as functions of leaf properties, vegetation structure, and micro-meteorological conditions. The model has been widely applied to enhance the understanding of remotely sensed data and canopy photosynthesis, and to support the quantitative use of reflectance and fluorescence for estimation of plant functional traits (Zhang et al., 2014; Damm et al., 2015; Van der Tol et al., 2016; Drusch et al., 2017).

The SCOPE model assumes that vegetation canopies are vertically homogeneous and horizontally infinite, as its radiative transfer routines are based on the classical 1-D SAIL model (Verhoef, 1984, 1985). However, in reality, canopies generally exhibit large vertical heterogeneity of both biophysical and biochemical properties (Dreccer et al., 2000; Valentinuz and Tollenaar, 2004; Ciganda et al., 2008). Vertical heterogeneity of chlorophyll and leaf water has been found in winter wheat (Liu et al., 2015; Zhao et al., 2017), corn (Ciganda et al., 2008) and beech tree (Wang and Li, 2013). A multi-layer structure of

* Corresponding author.
E-mail address: p.yang@utwente.nl (P. Yang).

http://dx.doi.org/10.1016/j.rse.2017.08.029
Received 1 March 2017; Received in revised form 8 August 2017; Accepted 21 August 2017

vegetation canopies is very common, for example, forests with a grass or bush layer, field crops with a weed layer and vegetation in the senescent stage (Kuusk, 2001; Verhoef and Bach, 2007; Ciganda et al., 2008; Liu et al., 2015).

The vertical heterogeneity in canopies has been included in some models, and simulations with these models show that its effect on top of canopy (TOC) reflectance is not negligible (Kuusk, 2001; Verhoef and Bach, 2007; Wang and Li, 2013). However, the effect of vertical heterogeneity on photosynthesis and fluorescence is unknown. It is expected that the vertical distribution of leaf properties can affect the light distribution in the canopy, and thereby fluorescence emission and photosynthesis of leaves. The vertical heterogeneity may also influence the re-absorption and scattering (radiative transfer) of the emitted fluorescence and thus directly affect TOC fluorescence. The simplification of vertically complex canopies to homogeneous canopies, with either mean values of phytometric and optical parameters of all leaves, or values of upper leaves, may lead to bias in the prediction of reflectance, fluorescence and photosynthesis by SCOPE. The inclusion of vertical heterogeneity of leaf properties in SCOPE will promote a better understanding of the link between remote sensing observations and plant functional traits.

This study presents a multi-layer reflectance, fluorescence and photosynthesis model based on SCOPE, called mSCOPE. The model mSCOPE considers the vertical variation of leaf biochemical and biophysical properties. The analytical solution of radiative transfer of the incident fluxes in SAIL (Verhoef, 1984) and the numerical solution of radiative transfer of the emitted fluorescence in SCOPE (Van der Tol et al., 2009) are not applicable in mSCOPE, because the assumption of the vertical homogeneity of canopy components (leaves) does not hold in mSCOPE. Therefore, we briefly introduce the theory of mSCOPE by giving the solutions of radiative transfer of incoming radiation and emitted fluorescence in multi-layer canopies. Several example simulations are presented to illustrate the effects of vertical heterogeneity of leaf chlorophyll and leaf water content on TOC reflectance, fluorescence and canopy photosynthesis. The model mSCOPE is also preliminary validated.

2. Description of mSCOPE

2.1. Overview

The model mSCOPE extends the 1-D model SCOPE for a homogeneous canopy to a vertically heterogeneous vegetation canopy. It has the same architecture of SCOPE: leaf and canopy RTMs combined with an energy balance model. At leaf level, Fluspect (Vilfan et al., 2016) is used to simulate leaf reflectance, transmittance, and fluorescence. At canopy level, RTMo and RTMf (Van der Tol et al., 2016), which are two SAIL based models, compute the radiative transfer of incident radiation and emitted fluorescence, respectively. All the four models (Fluspect, RTMo, RTMf, and the energy balance model) are internally connected. Fluspect provides necessary input for canopy RMTo and RMTf. RTMo predicts the distribution of irradiance and net radiation over surface elements (leaves and soil), which are inputs to the energy balance module and RTMf.

The model mSCOPE retains the assumption of homogeneity in the horizontal direction in SCOPE, but it incorporates vertical heterogeneity of leaf properties. The type of input parameters in mSCOPE is the same as in SCOPE (Table 1). The difference is that mSCOPE accepts different values of leaf properties for up to 60 layers (Table 2). In other words, the user is allowed to deviate from the default, uniform profile of the leaf properties, and specify vertical profiles. The operational efficiency of mSCOPE is similar to that of SCOPE, and the same output variables are generated.

2.2. Radiation fluxes

In order to calculate photosynthesis and fluorescence, the radiation distribution in the canopy is required. In mSCOPE, this is computed using the classical SAIL 4-stream theory. The radiative transfer of the direct solar flux (E_s), downward diffuse flux (E^-), upward diffuse flux (E^+) and flux in the viewing direction (E_o), is analytically represented by four linear equations:

$$\frac{dE_s}{Ldx} = kE_s \tag{1a}$$

$$\frac{dE^-}{Ldx} = -sE_s + aE^- - \sigma E^+ \tag{1b}$$

$$\frac{dE^+}{Ldx} = s'E_s + \sigma E^- - aE^+ \tag{1c}$$

$$\frac{dE_o}{Ldx} = wE_s + vE^- + v'E^+ - KE_o \tag{1d}$$

where x is the vertical relative height to the canopy bottom surface, and L is canopy LAI. The extinction coefficients (k and K) depend on canopy structural characteristics (i.e., LAI and leaf angle distribution) and sun-observer geometry. The scattering coefficients (s,a,σ,s',w,v,v') depend on canopy structural characteristics, sun-observer geometry and the optical characteristics (i.e., leaf reflectance ρ and transmittance τ) of foliar elements. These nine coefficients, first defined by Verhoef (1984), are given in Appendix A.

In mSCOPE, due to the consideration of vertical leaf properties heterogeneity, leaf reflectance, transmittance and the scattering coefficients may vary vertically. This has no impact on the extinction coefficients (K and k). Therefore, only the calculation of the diffuse fluxes (E^- and E^+) needs to be adapted in mSCOPE, while the calculation of the directional fluxes remains the same as in SCOPE (i.e., Eqs. (1a) and (1d)).

The vegetation layer's scattering matrix is given by

Table 1
Main input parameters of SCOPE.

Parameter	Explanation	Unit	Standard value	Range
C_{ab}	Chlorophyll $a+b$ content	$\mu g\ cm^{-2}$	40	0–100
C_{dm}	Leaf mass per unit area	$g\ cm^{-2}$	0.01	0–0.02
C_w	Equivalent water thickness	cm	0.015	0–0.05
C_s	Senescence material (brown pigments)	fraction	0.1	0–1
C_{ca}	Carotenoid content	$\mu g\ cm^{-2}$	10	0–30
N_l	Leaf structure parameter	-	1.5	1–3
LAI	Leaf area index	-	3	0–6
LIDFa	Leaf inclination function parameter a	-	−0.35	−1 to 1
LIDFb	Leaf inclination function parameter b	-	−0.15	−1 to 1
ϵ_1	Fluorescence efficiency of photosystem I	-	0.004	0–0.01
ϵ_2	Fluorescence efficiency of photosystem II	-	0.02	0–0.05
θ_s	Sun zenith angle	°	45	0–90
ψ	Relative azimuthal angle	°	0	0–360
PAR	Photosynthetically active radiation	$\mu mol\ m^{-2}s^{-1}$	1200	0–2200

Table 2
Extra input parameters of mSCOPE compared with SCOPE.

	mSCOPE				SCOPE
Layer index	1	2	…	N	
Leaf properties	$v(1)$	$v(2)$	…	$v(N)$	v_{canopy}
LAI	$L(1)$	$L(2)$	…	$L(N)$	L_{canopy}

Note: leaf properties parameters include C_{ab}, C_{dm}, C_w, C_s, C_{ca} and N_l.

$$\begin{bmatrix} \tau_{ss} & 0 & 0 & 0 \\ \tau_{sd} & \tau_{dd} & \rho_{dd} & 0 \\ \rho_{sd} & \rho_{dd} & \tau_{dd} & 0 \\ \rho_{so} & \rho_{do} & \tau_{do} & \tau_{oo} \end{bmatrix} = \begin{bmatrix} T_d & R_b \\ R_t & T_u \end{bmatrix} \tag{2}$$

where the subscripts attached to the vectors in the left matrix refer to the direct solar (s) flux, diffuse (d) flux and flux in the observer's (o) direction, and the subscripts attached to the right matrix denote downward (d), upward (u), top (t) and bottom (b). ρ_{x1x2} and τ_{x1x2} (i.e., $x1$ and $x2$ are s, d or o) are reflectance and transmittance of the layer for the case of flux $x1$ to flux $x2$. R_t and R_b are the reflectance at top and bottom of the vegetation layer, respectively. T_d and T_u are the downward and upward transmittance, respectively.

The vegetation layer is normally on top of a reflecting surface (e.g., soil). The surface bidirectional reflectance (R_{bottom}) is described by

$$\begin{bmatrix} R_{sd} & R_{dd} \\ R_{so} & R_{do} \end{bmatrix} = R_{bottom} \tag{3}$$

For a vertically homogeneous canopy (as in SCOPE), the analytical solution to the canopy scattering matrix (Eq. (2)) is first solved, then the TOC reflectance and flux profile are computed (Verhoef, 1984, 1985). However, for a vertically heterogeneous canopy (as in mSCOPE), it is difficult to get an analytical solution to the canopy scattering matrix: For each vegetation layer, the scattering matrix is different due to heterogeneous leaf properties. Therefore, in mSCOPE, we avoid the calculation of canopy scattering matrix. Instead, we developed a new strategy. The main idea comes from the adding method originally developed to simulate TOC reflectance in heterogeneous canopies (Cooper et al., 1982; Verhoef, 1985). In mSCOPE, we extended it to the calculation of the flux profile and TOC fluorescence.

The procedure is summarized as follows: 1. divide the vertical heterogeneous layer into several homogeneous layers; 2. start from the bottom homogeneous layer, calculate the surface reflectance of the combined system of the bottom surface (e.g., soil) and this layer; 3. add a new homogeneous vegetation layer above the surface of the previous system in step 2, and calculate the surface reflectance of the new system; 4. repeat step 3 until all homogeneous layers are added. 5. Once the surface reflectance at each vertical level is obtained, the fluxes profile can be computed from top to bottom, given the incident flux at top of the canopy.

In mSCOPE, the properties of a user defined N-layer canopy (where N < =60) are distributed over 60 sublayers. The use of 60 sublayers is similar to SCOPE, and it is necessary for computational reasons: Sufficiently thin sublayers of no more than 0.1 units of leaf area index (LAI) are needed to avoid problems in the numerical discretization of the differential equations. We use the term 'layers' for a layered canopy (such as understory and overstory), and the term 'sublayers' for the numerical discretization of the canopy.

In a heterogeneous 60-sublayer system that is bounded by a surface at the bottom, we distinguish the 60 sublayers by numbers from 1 to 60, and the fluxes at the bottom and the top of the system by the numbers 1 and 61. The levels at the interfaces between neighbouring sublayers are numbered from 2 to 60. Using this numbering for sublayers and their interfaces, the following set of equations describe radiative transfer in the whole system:

$$E^u(1) = R_{bottom}E^d(1) \tag{4a}$$

$$\begin{bmatrix} E^d(1) \\ E^u(2) \end{bmatrix} = \begin{bmatrix} t_d(1) & r_b(1) \\ r_t(1) & t_u(1) \end{bmatrix} \begin{bmatrix} E^d(2) \\ E^u(1) \end{bmatrix} \\ \vdots \tag{4b}$$

$$\begin{bmatrix} E^d(60) \\ E^u(61) \end{bmatrix} = \begin{bmatrix} t_d(60) & r_b(60) \\ r_t(60) & t_u(60) \end{bmatrix} \begin{bmatrix} E^d(61) \\ E^u(60) \end{bmatrix} \tag{4c}$$

where

$$E^d = \begin{bmatrix} E_s \\ E^- \end{bmatrix}; E^u = \begin{bmatrix} E^+ \\ E_o \end{bmatrix} \tag{5}$$

Except for the bottom reflectance R_{bottom}, all reflectance and transmittance matrices here refer to all the sublayers. These are therefore represented by lower case letters (i.e., t and r).

If only the downward fluxes at the top of the system are given, by the elements of the vector $E^d(61)$, all other flux vectors can be derived. To this end, we first solve the combination of the bottom with sublayer 1, which is given by the equations (i.e., from Eqs. (4a) and (4b))

$$E^u(1) = R_{bottom}E^d(1) \tag{6}$$

$$\begin{aligned} E^d(1) &= t_d(1)E^d(2) + r_b(1)E^u(1) \\ &= t_d(1)E^d(2) + r_b(1)R_{bottom}E^d(1) \\ &= [I - r_b(1)R_{bottom}]^{-1}t_d(1)E^d(2) \end{aligned} \tag{7}$$

$$\begin{aligned} E^u(2) &= r_t(1)E^d(2) + t_u(1)E^u(1) \\ &= r_t(1)E^d(2) + t_u(1)R_{bottom}E^d(1) \end{aligned} \tag{8}$$

Here we introduced a new quantity $X = (I - r_bR_{bottom})^{-1}t_d$, which is called the effective downward transmittance, since it describes the relationship between the downward fluxes at successive levels while taking into account the multiple reflections with the thick layer under the level of interest. Eqs. (7) and (8) are expressed as:

$$E^d(1) = X(1)E^d(2) \tag{9}$$

$$E^u(2) = [r_t(1) + t_u(1)R_{bottom}X(1)]E^d(2) \tag{10}$$

Eq. (10) gives the calculation of the upward flux at the top of sublayer 1. From Eq. (10), we obtain a new effective surface reflectance matrix at the top of sublayer 1, given by

$$R(2) = r_t(1) + t_u(1)R_{bottom}X(1) \tag{11}$$

In the following, we will use capital letters to indicate quantities that refer to all levels from the bottom (level 1) to the level of interest, and lower case letters to indicate quantities that only refer to a single thin sublayer. Thus, we may also identify R_{bottom} as $R(1)$, which is usually given as an input (e.g., soil reflectance).

In this way we obtain a recursive rule that can be extended up until the top of the whole system of sublayers. We use the equations

$$X(j) = [I - r_b(j)R(j)]^{-1}t_d(j) \tag{12}$$

$$R(j+1) = r_t(j) + t_u(j)R(j)X(j) \tag{13}$$

The matrices $X(j)$ are derived in Appendix B and written as

$$X(j) = \begin{bmatrix} \tau_{ss}(j) & 0 \\ \dfrac{\tau_{sd}(j) + \tau_{ss}(j)R_{sd}(j)\rho_{dd}(j)}{1 - \rho_{dd}(j)R_{dd}(j)} & \dfrac{\tau_{dd}(j)}{1 - \rho_{dd}(j)R_{dd}(j)} \end{bmatrix} = \begin{bmatrix} X_{ss}(j) & 0 \\ X_{sd}(j) & X_{dd}(j) \end{bmatrix} \tag{14}$$

The part $1/(1 - \rho_{dd}R_{dd})$ includes the repeated reflections of radiation between a surface and the bottom of a vegetation layer in the radiative transfer. By going from bottom to top, the final result obtained is the surface reflectance matrix at the top of all sublayers, $R(61)$.

After completion of the first loop, and since each X matrix connects the downward fluxes at level j to those at the next higher level $j+1$, we may start at the top level, for which the downward incident fluxes are given, and then derive the downward fluxes at all successive deeper levels by employing the previously stored X matrices. At the same time, one can derive the upward fluxes by using the stored R matrices. The equations used here are

$$E^d(j) = X(j)E^d(j+1) \tag{15}$$

$$E^u(j) = R(j)E^d(j) \tag{16}$$

With all scattering and extinction coefficients in Eq. 1 defined per unit of LAI, we can write for each sublayer with a small LAI (ΔL, 1/60 of

total canopy LAI). We can establish the scattering and extinction coefficients for all sublayers, and convert them into thin layer reflectances and transmittances:

$$\tau_{ss}(j) = 1 - k(j)\Delta L \tag{17a}$$

$$\tau_{dd}(j) = 1 - a(j)\Delta L \tag{17b}$$

$$\tau_{sd}(j) = s'(j)\Delta L \tag{17c}$$

$$\rho_{sd}(j) = s(j)\Delta L \tag{17d}$$

$$\rho_{dd}(j) = \sigma(j)\Delta L \tag{17e}$$

A complete algorithm to calculate the flux profile in a whole canopy layer of vertically heterogeneous vegetation is summarized as:

For sublayer $j = 1$ to 60 (bottom to top)

$$X_{ss}(j) = \tau_{ss}(j) \tag{18a}$$

$$X_{sd}(j) = \frac{\tau_{sd}(j)+\tau_{ss}(j)R_{sd}(j)\rho_{dd}(j)}{1-\rho_{dd}(j)R_{dd}(j)} \tag{18b}$$

$$X_{dd}(j) = \frac{\tau_{dd}(j)}{1-\rho_{dd}(j)R_{dd}(j)} \tag{18c}$$

$$R_{sd}(j+1) = \rho_{sd}(j) + \tau_{dd}(j)[R_{sd}(j)X_{ss}(j)+R_{dd}(j)X_{sd}(j)] \tag{18d}$$

$$R_{dd}(j+1) = \rho_{dd}(j) + \tau_{dd}(j)R_{dd}(j)X_{dd}(j) \tag{18e}$$

For sublayer $j = 60$ to 1 (top to bottom)

$$E_s(j) = X_{ss}(j)E_s(j+1) \tag{19a}$$

$$E^-(j) = X_{sd}(j)E_s(j+1) + X_{dd}(j)E^-(j+1) \tag{19b}$$

$$E^+(j) = R_{sd}(j)E_s(j) + R_{dd}(j)E^-(j) \tag{19c}$$

$E_s(61)$ and $E^-(61)$ refer to incident direct solar flux and diffuse flux, which are E_{sun} and E_{sky}. The hemispherical fluxes E^-, E^+ profiles and hemispherical reflectance factors R_{dd} and R_{sd} are computed.

2.3. The observed radiance

The adding method can be used to calculate the flux in the observer's direction E_o and the directional reflectance factors R_{so} and R_{do}. However, the hot spot effects on R_{so} and E_o are not considered in this method. Thus, R_{so} and E_o is given separately by solving Eq. (1d).

In a leaf canopy with finite leaf size the solar flux is described statistically, using the probability of sunshine and its complement, the probability of being in the shade. The probability of sunshine is described with a Poisson model as:

$$P_s(j) = e^{k\Delta L(j-60)} \tag{20}$$

The gap probability P_s controls the probability of sunshine. For example, at sunlit locations the solar flux equals to the solar flux incident at the top of the canopy, $E_s(61)$ or E_{sun} (i.e., incident direct solar flux). The probability for leaves in sublayer j (i.e., j from 1 to 60) or the soil (i.e., $j = 0$) of being observed through direct line-of-sight by an observer above the canopy is expressed by a similar function:

$$P_o(j) = e^{K\Delta L(j-60)} \tag{21}$$

The observed radiance contributed by the leaves is obtained by numerically solving Eq. (1d):

$$\begin{aligned} E_o^{leaves}(61)X &= \Delta L \sum_{j=1}^{60} [w(j)E_s(j)+v(j)E^-(j)+v'(j)E^+(j)]P_o(j) \\ &= \Delta L \sum_{j=1}^{60} [w(j)E_{sun}P_s(j)+v(j)E^-(j)+v'(j)E^+(j)]P_o(j) \\ &= \Delta L \sum_{j=1}^{60} \{w(j)E_{sun}P_s(j)P_o(j)+[v(j)E^-(j)+v'(j)E^+(j)]P_o(j)\} \end{aligned} \tag{22}$$

In order to take proper account of the hot spot effects, the product of the correlated probabilities P_sP_o, which indicates the joint probability of directly observing, through gaps in the canopy, sunlit phyto-elements or sunlit soil, must be replaced by the so-called bi-directional gap probability P_{so} (Verhoef, 1998; Van der Tol et al., 2009), which is given in Appendix C. Therefore we write

$$E_o^{leaves}(61) = \Delta L \sum_{j=1}^{60} \{w(j)E_{sun}P_{so}(j)+[v(j)E^-(j)+v'(j)E^+(j)]P_o(j)\} \tag{23}$$

The contribution from the soil is given by

$$E_o^{soil}(61) = E_{sun}P_{so}(0)R_{so}(1) + R_{do}(1)E^-(1)P_o(0) \tag{24}$$

where $R_{so}(1)$ and $R_{do}(1)$ are the directional reflectance factors of the background (R_{bottom}).

For the total TOC radiance (times π), we find in the general case

$$\pi L_o = E_o^{soil}(61) + E_o^{leaves}(61) \tag{25}$$

The reflectance of canopy observed by a sensor is given by

$$\rho = \frac{\pi L_o}{E_{sun}+E_{sky}} \tag{26}$$

where E_{sun} and E_{sky} are given as input or simulated from atmosphere radiative transfer models, such as MODTRAN (Berk et al., 2005).

The directional reflectance factors R_{so} and R_{do} are computed by using Eq. (26) setting E_{sky} or E_{sun} to 0 (i.e., when $E_{sky} = 0$, $\rho = R_{so}$).

2.4. Photosynthesis

Once the fluxes profile is computed, the radiation absorbed by the foliage can be calculated. The radiation absorbed by chlorophyll is used for photosynthesis, fluorescence and heat dissipation (Baker, 2008). Photosynthesis is then calculated as a product of the absorbed radiation and photosynthetic efficiency. The efficiencies of photosynthesis and fluorescence emission are simulated by a biochemical model as functions of the absorbed light, leaf temperature and CO_2 concentration and other factors (Van der Tol et al., 2014).

To calculate the total photosynthesis, the canopy has to be divided into multiple (e.g., 60 in mSCOPE) thin sublayers, as described in Section 2.2. Leaves in a thin sublayer are assumed to have the same ambient conditions including temperature and humidity, while the incident light on individual leaf in the thin layer may be different. Sunlit and shaded leaves are considered separately, in terms of the efficiencies of photosynthesis and fluorescence. For shaded leaves which are only illuminated by diffuse light, their efficiencies depend on their vertical relative height (j), expressed as $\epsilon_F(j)$ and $\epsilon_P(j)$. For sunlit leaves which are illuminated by both direct solar light and diffuse light, their efficiencies depend on their orientation (leaf zenith angle θ_l, azimuth angle φ_l) and vertical relative height (j), expressed as $\epsilon_F(j,\theta_l,\varphi_l)$ and $\epsilon_P(j,\theta_l,\varphi_l)$. Fluorescence and photosynthesis of the sunlit leaves are calculated for each specific leaf orientation. Numerically, 13 discrete leaf inclinations θ_l are used as in mSCOPE inherited from SCOPE and SAIL, and the uniform leaf azimuth φ_l distribution is also discretized to 36 angles of 5, 15,…, 355 ° relative to solar azimuth. At each sublayer, the leaf inclination distribution is described by using mathematical functions (LIDF) (De Wit, 1965) which quantify the probability of each leaf orientation class.

Canopy net photosynthesis (A, μmol CO_2 $m^{-2}s^{-1}$) is then expressed as:

$$A = \Delta L \sum_{j=1}^{60} \{[1-P_s(j)]\cdot A_h(j) + \sum_{36\varphi_l,13\theta_l} P_s(j)\cdot P(\varphi_l, \theta_l)\cdot A_s(j, \varphi_l, \theta_l)\} \quad (27)$$

where P_s is the probability of sunlit leaves and (1-P_s) is the probability of shaded leaves in sublayer j. $A_h(j)$ is the photosynthesis of shaded leaves in sublayer j per unit leaf area. $A_s(j,\varphi_l,\theta_l)$ is photosynthesis of sunlit leaves in sublayer j with the leaf orientation of (φ_l,θ_l) per unit leaf area. $P(\varphi_l,\theta_l)$ is the probability of leaves with given leaf orientation (φ_l,θ_l), which has 13 × 36 classes in the model. $P(\varphi_l,\theta_l)$ given by LIDF is identical for each sublayer in the canopy, because LIDF does not vary vertically in mSCOPE.

2.5. Fluorescence

Similar to SCOPE, the emission and radiative transfer of fluorescence are both modelled in mSCOPE. However, the vertical heterogeneity of leaf properties, have made the previous equations not applicable in this scenario. To account for this, new equations and solutions have been implemented in mSCOPE. To model the radiative transfer of fluorescence, we use a similar strategy as the adding method used in modelling of fluxes profile, described in section 2.2.

Fluorescence emitted by the foliage only consists of diffuse fluxes. Only radiative transfer of the upward and downward diffuse fluxes should be described. This can be established similarly to Eq. 4 and shown as follows.

$$E_F^-(j) = \tau_{dd}(j)E_F^-(j+1) + \rho_{dd}(j)E_F^+(j) + F_{em}^-(j) \quad (28a)$$

$$E_F^+(j) = \rho_{dd}(j)E_F^-(j+1) + \tau_{dd}(j)E_F^+(j) + F_{em}^+(j) \quad (28b)$$

where F_{em}^- and F_{em}^+ are the downward (' + ') and upward (' − ') diffuse hemispherical emitted fluorescence of a sublayer. They are excited by the direct solar flux (E_s), upward (E^+) and downward (E^-) diffuse light at each spectral band (λ_e) from 400 to 700 nm.

$$F_{em}^-(j) = \Delta L \int_{400}^{700} [s_f'(j)E_s(j+1) + \sigma_f'(j)E^-(j+1) + \sigma_f(j)E^+(j)]d\lambda_e \quad (29a)$$

$$F_{em}^+(j) = \Delta L \int_{400}^{700} [s_f(j)E_s(j+1) + \sigma_f(j)E^-(j+1) + \sigma_f'(j)E^+(j)]d\lambda_e \quad (29b)$$

where ΔL is LAI of a thin sublayer which is 1/60 of canopy LAI. The emission coefficients (with subscript f) are determined by sun-observer geometry, canopy structure, leaf optical properties and fluorescence emission efficiency of photosystems and given in Appendix A. The emission efficiencies in Eq. 29 are effective values for a sublayer, in which fluorescence emission is considered separately for sunlit and shaded leaves due to their different fluorescence emission efficiencies.

The flux at the top of an ensemble of sublayers may contain reflected downward flux as well as upward emitted flux, called U. Therefore we write

$$E_F^+(j) = R_{dd}(j)E_F^-(j) + U(j) \quad (30)$$

There is no upward emitted flux from the soil, thus $U(1) = 0$. For the reflection of fluorescence by the soil we write

$$E_F^+(1) = R_{dd}(1)E_F^-(1) \quad (31)$$

Substituting Eq. (30) into Eq. (28a) gives

$$E_F^-(j) = \frac{\tau_{dd}(j)E_F^-(j+1) + \rho_{dd}(j)U(j) + F_{em}^-(j)}{1-\rho_{dd}(j)R_{dd}(j)} \quad (32)$$

This can be written as

$$E_F^-(j) = X_{dd}(j)E_F^-(j+1) + Y(j) \quad (33)$$

where

$$Y(j) = \frac{\rho_{dd}(j)U(j) + F_{em}^-(j)}{1-\rho_{dd}(j)R_{dd}(j)} \quad (34)$$

Substituting Eq. (30) into Eq. (28b) we obtain

$$E_F^+(j+1) = \rho_{dd}(j)E_F^-(j+1) + \tau_{dd}(j)[R_{dd}(j)E_F^-(j) + U(j)] + F_{em}^+(j) \quad (35)$$

Substituting Eq. (33) into Eq. (35) we obtain

$$\begin{aligned} E_F^+(j+1) &= \rho_{dd}(j)E_F^-(j+1) + \tau_{dd}(j)\{R_{dd}(j)[X_{dd}(j)E_F^-(j+1) \\ &\quad + Y(j)] + U(j)\} + F_{em}^+(j) \\ &= [\rho_{dd}(j) + \tau_{dd}(j)R_{dd}(j)X_{dd}(j)]E_F^-(j+1) \\ &\quad + \tau_{dd}(j)[R_{dd}(j)Y(j) + U(j)] + F_{em}^+(j) \\ &= R_{dd}(j+1)E_F^-(j+1) + \tau_{dd}(j)[R_{dd}(j)Y(j) + U(j)] + F_{em}^+(j) \end{aligned} \quad (36)$$

Comparing Eq. (36) with Eq. (30), we obtain

$$U(j+1) = \tau_{dd}(j)[R_{dd}(j)Y(j) + U(j)] + F_{em}^+(j) \quad (37)$$

A complete algorithm to calculate the fluorescence profile in a vertically heterogeneous canopy is summarized as:

For sublayer j = 1 to 60 (bottom to top)

$$X_{dd}(j) = \frac{\tau_{dd}(j)}{1-\rho_{dd}(j)R_{dd}(j)} \quad (38a)$$

$$Y(j) = \frac{\rho_{dd}(j)U(j) + F_{em}^-(j)}{1-\rho_{dd}(j)R_{dd}(j)} \quad (38b)$$

$$R_{dd}(j+1) = \rho_{dd}(j) + \tau_{dd}(j)R_{dd}(j)X_{dd}(j) \quad (38c)$$

$$U(j+1) = \tau_{dd}(j)[R_{dd}(j)Y(j) + U(j)] + F_{em}^+(j) \quad (38d)$$

After application of these equations from the bottom to the top of the canopy, the following two equations can be applied to calculate the hemispherical fluorescence fluxes from top to bottom:

For sublayer j = 60 to 1 (top to bottom)

$$E_F^-(j) = X_{dd}(j)E_F^-(j+1) + Y(j) \quad (39a)$$

$$E_F^+(j) = R_{dd}(j)E_F^-(j) + U(j) \quad (39b)$$

Where $E_F^-(61) = 0$, $U(1) = 0$ and $R_{dd}(1)$ is given in the soil reflectance matrix.

2.6. The observed fluorescence

The fluorescence observed at top of canopy has four contributions: 1. fluorescence emitted by sunlit leaves and directly observed via $P_{so}(j)$, 2. fluorescence emitted by shaded leaves and directly observed via $P_o(j)$, 3. diffuse fluorescence flux scattered in the canopy and observed via $P_o(j)$, 4. diffuse fluorescence flux reflected by the soil and observed via $P_o(0)$.

Similar to Eq. 29, the emitted fluorescence for each sublayer is given as:

$$F_{em}^o(j) = \Delta L \int_{400}^{700} [w_f(j)E_s(j) + v_f(j)E^-(j) + v_f'(j)E^+(j)]d\lambda_e \quad (40)$$

The emitted fluorescence of sunlit leaves per unit layer $F_{em}^{so}(j)$ is distinguished from that of shaded leaves by $F_{em}^{ho}(j)$. The four contributions are given by

$$\pi L_F^1 = \sum_{j=1}^{60} F_{em}^{so}(j)P_{so}(j) \quad (41a)$$

$$\pi L_F^2 = \sum_{j=1}^{60} F_{em}^{ho}(j)[P_o(j) - P_{so}(j)] \quad (41b)$$

$$\pi L_F^3 = \sum_{j=1}^{60} [v(j)E_F^-(j) + v'(j)E_F^+(j)]P_o(j) \quad (41c)$$

Table 3
Input parameters of vertical leaf chlorophyll (C_{ab}, μg cm^{-2}) and equivalent water thickness (C_w, cm) profile in six two-layer canopy scenarios.

Scenario	Upper layer		Lower layer	
	C_{ab}	C_w	C_{ab}	C_w
S0	40	0.015	40	0.015
S1	60	0.02	20	0.01
S2	20	0.01	60	0.02
S3	40	0.015	0	0.01
S4	40	0.015	20	0.02
S5	40	0.015	60	0.03

$$\pi L_F^4 = E_F^-(1) R_{do}(1) P_o(0) \tag{41d}$$

The total observed fluorescence (L_F) is summed by:

$$L_F = L_F^1 + L_F^2 + L_F^3 + L_F^4 \tag{42}$$

3. Materials and methods

3.1. Synthetic dataset of two-layer canopies

First, synthetic datasets were used to evaluate the vertical heterogeneity effect on TOC fluorescence, TOC reflectance and canopy photosynthesis. In the current experiment, scenarios for two-layer canopies have been simulated. A two-layer canopy is one of the simplest multilayer canopies and it has also been used in several heterogeneous reflectance models, including the two-layer canopy reflectance model (Kuusk, 2001) and 4SAIL2 (Verhoef and Bach, 2007).

Specifically, six scenarios were generated from different combinations of leaf chlorophyll C_{ab} and leaf water content C_w (Table 3). These six scenarios can be considered as two groups of canopies. In the first group, the three scenarios (S0, S1, S2) had the same canopy averaged C_{ab} and C_w, which were 40 μg cm^{-2} and 0.015 cm, respectively, while the vertical distributions of C_{ab} and C_w were different. In the second group, the four scenarios (S0, S3, S4, S5) had the same C_{ab} and C_w of leaves in the upper layer, while C_{ab} and C_w varied in the lower layer. In all the scenarios, LAI of both two layers was 1.5 (total canopy LAI was 3). The other model parameters were set to the 'standard' values (Table 1). It should be noted that S0 was a scenario of homogeneous canopy that served as a reference.

3.2. Field measurement dataset of corn canopy

To further investigate the effects of vertical heterogeneity, reflectance, fluorescence and photosynthesis were simulated with field measured data as input. The field experimental data was acquired from a corn canopy, where synchronous seasonal measurements of vertical profiles of leaf chlorophyll content and LAI, TOC reflectance from 400 to 900 nm were available (Gitelson et al., 2003; Gitelson et al., 2006; Ciganda et al., 2008). The measurements on 3 days in the early, middle and end of the growing season were selected, which were on DOY (day of year) 173, 206 and 259 in 2005, as shown in Figs. 1 and 2.

We first approximated the canopy structure and leaf properties from TOC reflectance by inverting the reflectance calculating routine in RTMo of SCOPE. The numerical optimization method (Nocedal and Wright, 2006) was used to retrieve the parameters C_{ab}, C_{dm}, C_w, C_s, C_{ca}, N_l, LIDFa and LIDFb by minimizing a cost function:

$$C = \sum_{i=1}^{n} [R_m(i) - R_s(i)]^2 \tag{43}$$

where R_m and R_s were measured and simulated TOC reflectance, and i represented a band in the reflectance measurements. In the retrieval, LAI was fixed to the measured canopy LAI, which was 1.63, 5.23 and 3.77 on the three days.

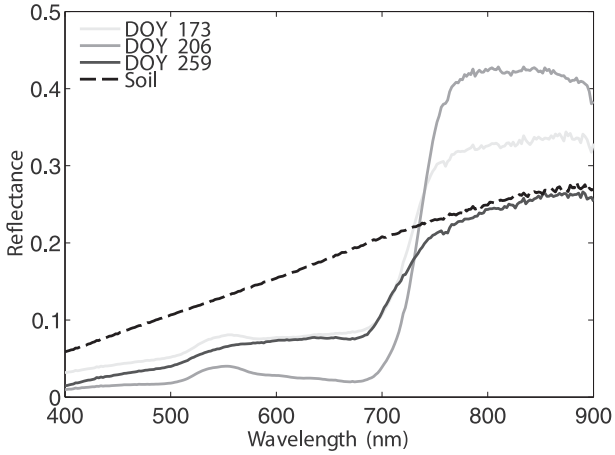

Fig. 1. Canopy reflectance observations on DOY 173, 206 and 259 in the growing season and soil reflectance (DOY, day of year).

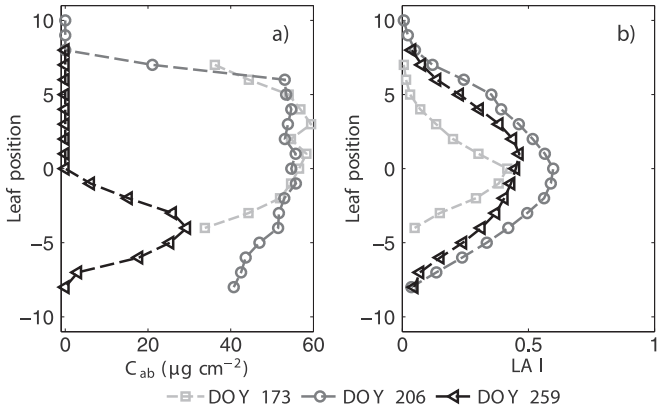

Fig. 2. Vertical profile of leaf chlorophyll content (C_{ab}) and LAI in the field datasets acquired on three days in the corn growing season. (Note, y axis represents leaf position. The collar or ear leaf was labelled as leaf 0. The leaves above or below leaf 0 were identified with a '+' or '−' sign, respectively, with the corresponding position number. For example, the first leaf above the collar or ear leaf was identified as +1, the first leaf below the collar or ear leaf was identified as −1; DOY, day of year).

Reflectance, fluorescence and photosynthesis were simulated for each canopy from both SCOPE and mSCOPE. In the SCOPE simulation, the retrieved parameters were used except for chlorophyll content, for which canopy mean values measured (50.2, 41.2, 7.8 μg cm^{-2}) were used. In the mSCOPE simulations, the measured leaf chlorophyll profiles and the retrieved canopy 'effective' values of other properties were used as input. The canopy had 12, 17 and 19 leaves on DOY 173, DOY 206 and DOY 259, respectively. Chlorophyll of each leaf was measured (Fig. 2). Regardless of the different vertical complexity of the corn canopy on three days, the vertical profiles of C_{ab} of the canopy were implemented in mSCOPE in three ways, notably with 3, 7, and 11 layers. Leaves that had similar values of chlorophyll content were merged into one layer and the mean chlorophyll content of the leaves was assigned to the merged layer. Incident PAR was set to 1200 μmol m^{-2}s^{-1} as shown in Table 1.

3.3. Evaluation and validation

The simulation results of the six scenarios in the synthetic dataset were compared to evaluate how the vertical heterogeneity of chlorophyll and water content affects the canopy reflectance, fluorescence and photosynthesis. First, simulated TOC reflectance (nadir, 400–2400 nm) and TOC fluorescence (nadir, 650–850 nm) from S1 to S5 were visually compared to the homogeneous scenario S0. Then, one

visible band (550 nm) and one near-infrared water absorption band (1200 nm) were selected for quantitative evaluation. Fluorescence at 687 nm and 760 nm (F_{687} and F_{760}) were also compared, representing the red and far-red fluorescence used in remote sensing of vegetation (Meroni et al., 2009; Rascher et al., 2015). Further, simulations of net photosynthesis, absorbed photosynthetically active radiation (aPAR) and photosynthetic light use efficiency (LUE = A/aPAR) were compared and evaluated. SCOPE and mSCOPE were crossed validated by comparing their respective simulation results of the homogeneous scenario.

For the field corn dataset, simulations of TOC reflectance from mSCOPE were compared with the field measurements, to validate the accuracy of mSCOPE. Also, simulation results from mSCOPE were compared with results from SCOPE, to evaluate the effects of vertical distributions of C_{ab} on TOC reflectance, fluorescence and canopy net photosynthesis.

4. Results

4.1. Simulation results of synthetic two-layer canopies

TOC reflectance, TOC fluorescence and canopy photosynthesis of the six synthetic scenarios were simulated from mSCOPE. The results of the heterogeneous scenarios (S1–S5) and the comparison reference homogeneous scenario (S0) are shown in Fig. 3.

Modelled reflectance was different for each group-1 scenario (S0, S1 and S2), despite having equal total canopy C_{ab} and C_w (Fig. 3a). The difference was especially obvious in the visible region from 400 to 700 nm. Modelled reflectance also varied significantly among group-2 scenarios (S0, S3, S4 and S5), where upper layer had the same C_{ab} and C_w while lower layer C_{ab} and C_w increased from S3 to S5. The differences were obvious in both the visible and infrared region (700–2400 nm). Especially, the disparity of infrared reflectance among group-2 scenarios was much higher than the disparity among group-1 scenarios. Simulated reflectance was clearly the highest in S3 among the group-2 scenarios. Reflectance at 550 nm of S3, S4 and S5 differed by 34%, 9% and 5% respectively, compared with the reflectance of the homogeneous canopy S0, and reflectance at 1200 nm differed by 2%, 2% and 6%, respectively.

Fluorescence of the six scenarios also varied (Fig. 3c and Fig. 3d). In group-1 scenarios, at 687 nm (F_{687}), S1 and S2 differed 3% and 10% respectively, compared to the homogeneous canopy S0; while at 760 nm(F_{760}), the difference of S1, S2 with S0 is marginal. In group-2 scenarios, at 687 nm (F_{687}), S3, S4, and S5 differed 23%, 7%, and 2% respectively, compared to the homogeneous canopy S0; while at 760 nm (F_{760}), the difference to S0 was 33%, 6% and 2% respectively.

Table 4
Photosynthetically active radiation absorbed (aPAR), net photosynthesis (A) and light use efficiency (LUE) simulated from mSCOPE of the six synthetic scenarios.

Scenario	aPAR	A	LUE
	(μmol m^{-2}s^{-1})	(μmol CO$_2$ m^{-2}s^{-1})	(mol CO$_2$ mol^{-1}photon)
S0	943.02	25.17	0.027
S1	973.07	25.07	0.026
S2	842.40	24.78	0.030
S3	788.28	20.47	0.026
S4	922.50	24.85	0.027
S5	951.64	25.28	0.027

The results of net photosynthesis (A), absorbed photosynthetically active radiation (aPAR) by all phyto-elements and light use efficiency (LUE = A/aPAR) varied in the six scenarios (Table 4). In group-1 scenarios (S0, S1 and S2), canopies with the same total C_{ab} and C_w had a similar photosynthesis, but different aPAR and LUE. The S1 canopy absorbed more light than the S0 and S2 canopies, but had the smallest LUE. In group-2 scenarios (S0, S3, S4 and S5), aPAR and A increased with increasing total C_{ab}, but differences among scenarios in LUE were minor.

4.2. Simulated and measured results of field corn canopy

The retrievals of canopy structure and leaf properties from measured reflectance (Table 5) show that the relative senescence material C_s of corn was 0 in the early and middle growing season (DOY 173, DOY 206), but 0.4 in the senescent stage (DOY 259). Both leaf water content (C_w) and carotenoid content (C_{ca}) were the lowest on DOY 259. The retrieved C_{ab} was close to measured canopy mean C_{ab} on DOY 173 and 206 (50.2 and 41.2 μg cm^{-2}), but it was three times as high as measured canopy mean C_{ab} on DOY 259 (7.5 μg cm^{-2}).

The retrieved values (except C_{ab}) were further input into mSCOPE and SCOPE for forward simulations. Modelled TOC reflectance and fluorescence from mSCOPE and SCOPE, as well as measured TOC reflectance are presented in Fig. 4, and simulated photosynthesis in Table 6. SCOPE and mSCOPE (3, 7 or 11 layers) produced similar reflectance simulations, and they were all close to the measured

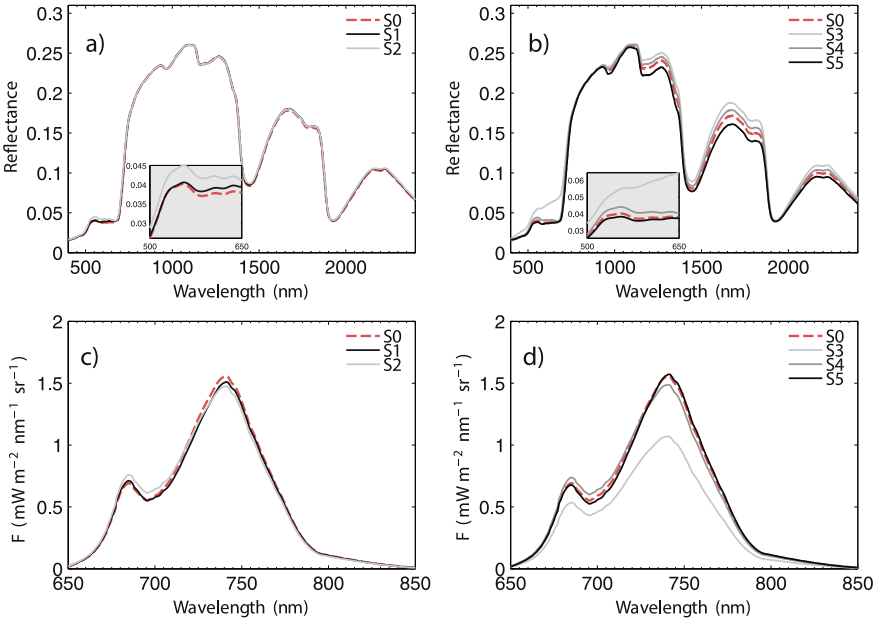

Fig. 3. Simulation results for the six synthetic scenarios from mSCOPE. a), b) nadir reflectance spectra; c), d) nadir fluorescence spectra (Note, S0 is a homogeneous scenario, S1–S5 have different vertical distribution of chlorophyll content (C_{ab}) and leaf water content (C_w)). Reflectance spectra from 500 to 650 nm were enlarged in the grey boxes.

Table 5
The parameters of canopy structure and leaf properties of the corn canopy retrieved from the TOC reflectance measurements.

Parameter	DOY 173	DOY 206	DOY 259
C_{dm} (g cm^{-2})	0.01	0.04	0.005
C_w (cm)	0.04	0.05	0.01
C_s	0	0	0.4
N_l	1.5	1.7	1.4
C_{ca} (μg cm^{-2})	5.6	3.7	1.4
C_{ab} (μg cm^{-2})	55	38	25
LIDFa	−0.79	−0.97	−1
LIDFb	0.21	0.03	0

Table 6
Net photosynthesis simulated from mSCOPE and SCOPE of the corn canopy on the three days.

	Photosynthesis (μmol CO_2 m^{-2}s^{-1})		
	DOY 173	DOY 206	DOY 259
SCOPE	23.8	37.7	27.9
mSCOPE-3	23.9	37.1	6.7
mSCOPE-7	23.9	37.0	5.9
mSCOPE-11	23.9	37.0	5.9

reflectance on both DOY 173 and DOY 206. However, the simulations for DOY 259 diverged. Compared to SCOPE, mSCOPE performed much better in terms of reflectance simulation in the visible spectral region. Reflectance from SCOPE was clearly lower than reflectance from mSCOPE in the range of 570 to 700 nm. However, fluorescence (650 to 850 nm) from SCOPE was much higher than fluorescence from mSCOPE at DOY 259. The number of layers in mSCOPE had negligible impact on the modelling results. Simplification of the corn canopy into 3, 7 or 11 layers, all produced similar fluorescence. Photosynthesis simulation with SCOPE and mSCOPE were very similar for DOY 173 and DOY 206. Howver, a notable difference was found in the results on DOY 259, when the homogeneous SCOPE model produced a much higher (more than threefold) photosynthesis than mSCOPE.

5. Discussion

5.1. Model validation

The performance of mSCOPE has been tested in two ways: by analysing the differences with SCOPE, and by comparing simulated to measured reflectance of corn. For a homogeneous canopy, SCOPE and mSCOPE produce identical output (results not shown). If the vertical heterogeneity of the canopy is limited, such as in the corn canopy data used in this study on DOY 173 and DOY 206, then mSCOPE and SCOPE produce very similar reflectance, fluorescence and photosynthesis simulations.

5.2. Effects of vertical heterogeneity on TOC reflectance, fluorescence and photosynthesis

The modelled results from the six synthetic scenarios showed noticeable effect of vertical heterogeneity on canopy TOC reflectance, which confirms findings in previous modelling studies (Kuusk, 2001; Widlowski et al., 2007; Wang and Li, 2013; Zhao et al., 2017). Furthermore, significant effect of canopy heterogeneity on simulated TOC fluorescence and photosynthesis was demonstrated in this study (Fig. 3c, 3d). TOC reflectance and fluorescence vary with different vertical distribution of C_{ab} and C_w, even if the canopies have the same total C_{ab} and C_w (Fig. 3a and 3c). The lower leaves in a canopy with LAI = 3 still has a noticeable impact on TOC reflectance and fluorescence (Fig. 3b and 3d). It is worth noting that canopy openness plays an important role in relative contribution of upper and leaves in the canopy signal (Martens et al., 1993; Chen and Cihlar, 1995; Nascimento et al., 2007). The lower leaves in canopies with low LAI have a better chance (P_o in Eq. (21)) to be observed than those with high LAI.

The differences in fluorescence were mainly caused by the distribution of C_{ab}, and the effect of C_w was very small. Different C_{ab} distribution led to different aPAR (Jacquemoud et al., 2009), resulting in different fluorescence emission. The effects of vertical heterogeneity of leaf properties on the fluorescence appear to be wavelength-dependent. F_{760} and F_{687} varied differently among the synthetic scenarios (Fig. 3d). This wavelength dependence is caused by reabsorption: F_{687} has higher re-absorption and lower scattering than F_{760}.

The results of the corn canopy demonstrate that neglecting vertical

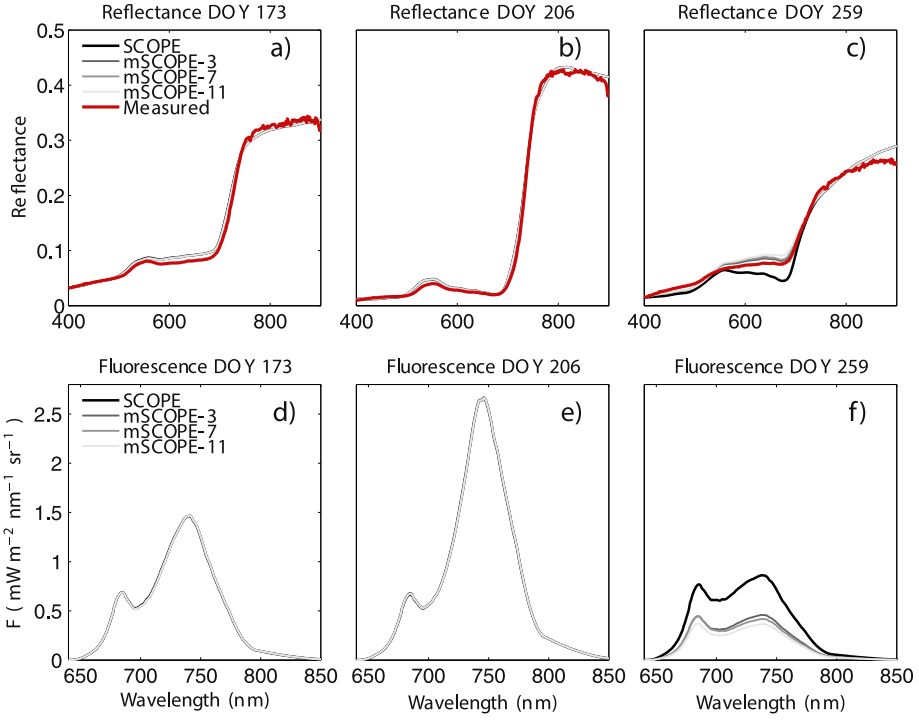

Fig. 4. Simulation results of the corn canopy on three days in the growing season. Upper panel: comparison among measured, mSCOPE modelled, and SCOPE modelled reflectance; lower panel: comparison between mSCOPE modelled and SCOPE modelled fluorescence (Note: the vertical profile of C_{ab} for each canopy was simplified as 3, 7, and 11 layers and implemented in mSCOPE. DOY, day of year).

heterogeneity of C_{ab} may lead to significant biases in prediction of TOC reflectance, fluorescence and canopy photosynthesis in the senescent stage. The biases of vegetation models as a result of simplifications depend on the complexity of the canopies in reality, which was also demonstrated for TOC reflectance by Wang and Li (2013). In the senescent stage of crops, canopies usually have large vertical heterogeneity of leaf properties (Verhoef and Bach, 2007; Ciganda et al., 2008; Liu et al., 2015). Compared to SCOPE, mSCOPE provided a closer prediction of TOC reflectance to the field measurement in the visible region due to the consideration of the vertical heterogeneity of C_{ab} (Fig. 4c). SCOPE produced considerably higher estimates of both fluorescence and photosynthesis in the senescent stage when average C_{ab} is used as input (Fig. 4f and Table 6) compared to mSCOPE. Although simulations of a multi-layer canopy are different from a single layer canopy, the number of layers does not need to be large: The three simplifications in mSCOPE (mSCOPE-3, mSCOPE-7 and mSCOPE-11) yield similar results. Thus, the three-layer simplification (mSCOPE-3) appears a sufficiently detailed representation of the vertical heterogeneity of the senescent corn, and adding layers does not affect the results significantly in this case. The fact that three layers is sufficient may be due to the ' bell-shape' profiles (Ciganda et al., 2008) of chlorophyll (Fig. 2), which can easily be approximated by three layers. However, a single layer as in SCOPE may be an oversimplification.

From the above analysis, the effects of considering canopy vertical heterogeneity on reflectance, fluorescence and photosynthesis have been demonstrated. However, our experimental setup was rather simple compared to complex canopies in reality. In the synthetic scenarios, two layer canopies were generated, and only C_{ab} and C_w were varied vertically. In the corn canopy, only vertical variation of C_{ab} was considered. The lack of measurements of fluorescence and photosynthesis of the corn canopies also limited the validation of the full model. Since the main focus of this paper is to introduce the mSCOPE model, only a simplified validation and evaluation were conducted.

5.3. Implications

The model mSCOPE is an extension of SCOPE to include canopy vertical heterogeneity of leaf biophysical and biochemical properties. It simulates reflectance, fluorescence and photosynthesis of multi-layer canopies. Vegetation reflectance models for heterogeneous canopies have been developed. There are two-layer (Kuusk, 2001), multi-layer (Wang and Li, 2013) and 3-D models, such as DART (Gastellu-Etchegorry et al., 1996) and Raytran (Govaerts and Verstraete, 1998). DART recently included the fluorescence simulation (Gastellu-Etchegorry et al., 2017) to promote a better understanding of remote sensed signals and plant physiology. The model mSCOPE benefits from the original SCOPE model which incorporates the energy balance model. The energy balance model allows predicting the response of vegetation to the ambient conditions, such as temperature and humidity (Van der Tol et al., 2014).

The adding concept applied in mSCOPE has potential in radiative transfer modelling. It was originally used for the calculation of TOC reflectance (Cooper et al., 1982; Verhoef, 1985). We have extended the adding method to the calculation of vertical flux profiles incorporating the radiation emission (fluorescence) in multi-layer canopies. These have been summarized in Eqs. 18, 19 and in Eqs. 38, 39 (with fluorescence emission). Our approach can be applied in mediums other than vegetation, such as water and atmosphere which have a clear multi-layer structure. Moreover, it can also be used for the calculation of thermal fluxes in various mediums as similar to the calculation of fluorescence fluxes. The detailed mathematical explanation in Section 2 will allow applying our approach in the potential applications mentioned above.

6. Conclusion

Vegetation canopies generally exhibit vertical heterogeneity in leaf properties. Homogeneous models are in some cases insufficient in their representation of the canopy for understanding the remote sensing signal of reflectance, fluorescence and canopy photosynthesis. An integrated model of radiative transfer and energy balance that addresses vertical heterogeneity of leaf biophysical and biochemical parameters within the canopy has been proposed. The model mSCOPE simulates TOC reflectance, fluorescence and photosynthesis, for vertically heterogeneous canopies. It could provide a better understanding of remote sensing signals and plant physiology.

Acknowledgements

This work of the first author (Peiqi Yang) was supported by the China Scholarship Council (CSC) under grant 201406040058. The authors thank CALMIT, School of Natural Resources, University of Nebraska – Lincoln for providing the experimental data and Jing Liu for assistance in writing the manuscript. Fruitful exchange of ideas has taken place at workshop funded by ESSEM Cost Action 1309 'OPTIMISE'. We thank the editor and anonymous reviewers for their constructive feedback and the chance to improve the quality of our manuscript accordingly.

Appendix A. Extinction, scattering and emission coefficients

Leaf reflectance and transmittance (ρ and τ) are simulated by leaf RTMs (i.e., FLUSPECT in mSCOPE). The reflectance of both the adaxial and abaxial sides of leaves is assumed to the same in the model. Leaf angle is characterized by leaf zenith angle (θ_l) and azimuth angle (φ_l). Numerically, 13 discrete leaf inclinations are used as in mSCOPE inherited from SCOPE and SAIL, and the uniform leaf azimuth distribution is now also discretized to 36 angles of 5, 15,…, 355° relative to solar azimuth. The leaf inclination distribution is described by using mathematical functions (LIDF) (De Wit, 1965) which quantifies the probability of each leaf orientation class. Sun-observer geometry is determined by the sun and observer's zenith angle (θ_s and θ_o), and the relative azimuth angle (ψ, the absolute difference between their azimuth angles). The coefficients are expressed as follows:

$$f_s = \cos\theta_l + \tan\theta_s \sin\theta_l \cos\varphi_l \tag{A.1a}$$

$$f_o = \cos\theta_l + \tan\theta_o \sin\theta_l \cos(\varphi_l - \psi) \tag{A.1b}$$

$$k = |f_s| \tag{A.1c}$$

$$K = |f_o| \tag{A.1d}$$

$$s = \frac{1}{2}[|f_s|(\rho+\tau)+f_s \cos\theta_l(\rho-\tau))] \tag{A.1e}$$

$$s' = \frac{1}{2}[|f_s|(\rho+\tau)-f_s \cos\theta_l(\rho-\tau))] \tag{A.1f}$$

$$\sigma = \frac{1}{2}[(\rho+\tau)+(\rho-\tau))\cos^2\theta_l] \tag{A.1g}$$

$$a = 1 - \frac{1}{2}[(\rho+\tau)-(\rho-\tau))\cos^2\theta_l] \tag{A.1h}$$

$$v = \frac{1}{2}[|f_o|(\rho+\tau)+f_o\cos\theta_l(\rho-\tau))] \tag{A.1i}$$

$$v' = \frac{1}{2}[|f_o|(\rho+\tau)-f_o\cos\theta_l(\rho-\tau))] \tag{A.1j}$$

$$w = \frac{1}{2}[|f_s f_o|(\rho+\tau)+f_s f_o(\rho-\tau))]. \tag{A.1k}$$

The nine emission coefficients (those with subscripts of f) are determined both by sun-leaf-observer geometry, which is characterized by the zenith angles of the sun (θ_s), leaf (θ_l) and observer (θ_o), the leaf azimuth angle (φ_l) and the relative azimuth angles between the sun and the observer (ψ), and by the leaf excitation-emission matrices at the backward and forward side (M_b and M_f) (Vilfan et al., 2016). For individual leaves, they are given by

$$f_s = \cos\theta_l + \tan\theta_s \sin\theta_l \cos\varphi_l \tag{A.2a}$$

$$f_o = \cos\theta_l + \tan\theta_o \sin\theta_l \cos(\varphi_l - \psi) \tag{A.2b}$$

$$s_f = \frac{1}{2}[|f_s|(M_b+M_f)+f_s\cos\theta_l(M_b-M_f)] \tag{A.2c}$$

$$s_f' = \frac{1}{2}[|f_s|(M_b+M_f)-f_s\cos\theta_l(M_b-M_f)] \tag{A.2d}$$

$$\sigma_f = \frac{1}{2}[(M_b+M_f)+(M_b-M_f)\cos^2\theta_l] \tag{A.2e}$$

$$\sigma_f' = \frac{1}{2}[(M_b+M_f)-(M_b-M_f)\cos^2\theta_l] \tag{A.2f}$$

$$v_f = \frac{1}{2}[|f_o|(M_b+M_f)+f_o\cos\theta_l(M_b-M_f)] \tag{A.2g}$$

$$v_f' = \frac{1}{2}[|f_o|(M_b+M_f)-f_o\cos\theta_l(M_b-M_f)] \tag{A.2h}$$

$$w_f = \frac{1}{2}[|f_s f_o|(M_b + M_f) + f_s f_o(M_b - M_f)]. \tag{A.2i}$$

The excitation-emission matrices (M_b and M_f) are functions of fluorescence emission efficiency and thus are determined by the net radiation. It is noted that the matrices are dependent on the illumination conditions of the individual leaf.

Appendix B. Effective downward transmittance X

$$\begin{aligned} I-r_b R &= \begin{bmatrix}1 & 0\\ 0 & 1\end{bmatrix} - \begin{bmatrix}0 & 0\\ \rho_{dd} & 0\end{bmatrix}\begin{bmatrix}R_{sd} & R_{dd}\\ R_{so} & R_{do}\end{bmatrix} \\ &= \begin{bmatrix}1 & 0\\ 0 & 1\end{bmatrix} - \begin{bmatrix}0 & 0\\ \rho_{dd}R_{sd} & \rho_{dd}R_{dd}\end{bmatrix} \\ &= \begin{bmatrix}1 & 0\\ -\rho_{dd}R_{sd} & 1-\rho_{dd}R_{dd}\end{bmatrix} \end{aligned} \tag{B.1}$$

Therefore, we find

$$(I - r_b R)^{-1} = (1 - \rho_{dd}R_{dd})^{-1}\begin{bmatrix}1-\rho_{dd}R_{dd} & 0\\ \rho_{dd}R_{sd} & 1\end{bmatrix} \tag{B.2}$$

Post-multiplication by t_d then gives

$$\begin{aligned} X &= (I-r_b R)^{-1} t_d \\ &= (1-\rho_{dd}R_{dd})^{-1}\begin{bmatrix}1-\rho_{dd}R_{dd} & 0\\ \rho_{dd}R_{sd} & 1\end{bmatrix}\begin{bmatrix}\tau_{ss} & 0\\ \tau_{sd} & \tau_{dd}\end{bmatrix} \\ &= \begin{bmatrix}\tau_{ss} & 0\\ \dfrac{\tau_{sd}+\tau_{ss}R_{sd}\rho_{dd}}{1-\rho_{dd}R_{dd}} & \dfrac{\tau_{dd}}{1-\rho_{dd}R_{dd}}\end{bmatrix} \end{aligned} \tag{B.3}$$

where only R_{sd} and R_{dd} refer to thick layer extending from the bottom to level j, which means that one can write

$$X(j) = \begin{bmatrix}\tau_{ss}(j) & 0\\ \dfrac{\tau_{sd}(j)+\tau_{ss}(j)R_{sd}(j)\rho_{dd}(j)}{1-\rho_{dd}(j)R_{dd}(j)} & \dfrac{\tau_{dd}(j)}{1-\rho_{dd}(j)R_{dd}(j)}\end{bmatrix} = \begin{bmatrix}X_{ss}(j) & 0\\ X_{sd}(j) & X_{dd}(j)\end{bmatrix} \tag{B.4}$$

Appendix C. Bi-directional gap probability

For sublayer j, the vertical relative coordinate is given by

$$x = (j - 60)/60 \tag{C.1}$$

and the bi-directional gap probability of the sublayer is given by Verhoef (1998)

$$P_{so}(j) = \exp\left\{(K+k)x + \sqrt{Kk}\frac{s_l}{a}[1-\exp(xa/s_l)]\right\} \tag{C.2}$$

where s_l is the hot spot size parameter, approximated as

$$s_l = \frac{w_l}{h}\frac{2}{K+k} \tag{C.3}$$

where w_l is the average leaf width and h canopy height, and the factor $2/(K + k)$ accomplishes a correction for leaf projection area on a horizontal plane. The function a depends only on the sun-target-sensor angular geometry, and is given by

$$a = \sqrt{\tan^2\theta_s + \tan^2\theta_o - 2\tan\theta_s\tan\theta_o\cos\psi} \tag{C.4}$$

References

Baker, N.R., 2008. Chlorophyll fluorescence: a probe of photosynthesis in vivo. Annu. Rev. Plant Biol. 59, 89–113.

Berk, A., Anderson, G.P., Acharya, P.K., Bernstein, L.S., Muratov, L., Lee, J., Fox, M., Adler-Golden, S.M., Chetwynd, J.H., Hoke, M.L., et al., 2005. MODTRAN 5: a reformulated atmospheric band model with auxiliary species and practical multiple scattering options: update. In: Defense and Security. International Society for Optics and Photonics, pp. 662–667.

Chen, J.M., Cihlar, J., 1995. Plant canopy gap-size analysis theory for improving optical measurements of leaf-area index. Appl. Opt. 34 (27), 6211–6222.

Ciganda, V., Gitelson, A., Schepers, J., 2008. Vertical profile and temporal variation of chlorophyll in maize canopy: quantitative crop vigor indicator by means of reflectance-based techniques. Agric. J. 100 (5), 1409–1417.

Collatz, G.J., Ribas-Carbo, M., Berry, J., 1992. Coupled photosynthesis-stomatal conductance model for leaves of C4 plants. Funct. Plant Biol. 19 (5), 519–538.

Cooper, K., Smith, J., Pitts, D., 1982. Reflectance of a vegetation canopy using the adding method. Appl. Opt. 21 (22), 4112–4118.

Damm, A., Guanter, L., Paul-Limoges, E., Van der Tol, C., Hueni, A., Buchmann, N., Eugster, W., Ammann, C., Schaepman, M., 2015. Far-red sun-induced chlorophyll fluorescence shows ecosystem-specific relationships to gross primary production: an assessment based on observational and modeling approaches. Remote Sens. Environ. 166, 91–105.

De Wit, C., 1962. Space relationships within populations of one or more species.

De Wit, C.T., 1965. Photosynthesis of leaf canopies. In: Agricultural Research Report. Pudoc.

Dreccer, M., Van Oijen, M., Schapendonk, A., Pot, C., Rabbinge, R., 2000. Dynamics of vertical leaf nitrogen distribution in a vegetative wheat canopy. Impact on canopy photosynthesis. Ann. Bot. 86 (4), 821–831.

Drusch, M., Moreno, J., Del Bello, U., Franco, R., Goulas, Y., Huth, A., Kraft, S., Middleton, E.M., Miglietta, F., Mohammed, G., et al., 2017. The FLuorescence EXplorer mission concept-ESA's earth explorer 8. IEEE Trans. Geosci. Remote Sens. 55 (3), 1273–1284.

Farquhar, G.D., von Caemmerer, S.v., Berry, J., 1980. A biochemical model of photosynthetic CO2 assimilation in leaves of C3 species. Planta 149 (1), 78–90.

Gastellu-Etchegorry, J.-P., Demarez, V., Pinel, V., Zagolski, F., 1996. Modeling radiative transfer in heterogeneous 3-D vegetation canopies. Remote Sens. Environ. 58 (2), 131–156.

Gastellu-Etchegorry, J.-P., Lauret, N., Yin, T., Landier, L., Kallel, A., Malenovskỳ, Z., Al Bitar, A., Aval, J., Benhmida, S., Qi, J., et al., 2017. Dart: recent advances in remote sensing data modeling with atmosphere, polarization, and chlorophyll fluorescence. IEEE J. Sel. Top. Appl. Earth Obs. Remote Sens.

Gitelson, A.A., Gritz, Y., Merzlyak, M.N., 2003. Relationships between leaf chlorophyll content and spectral reflectance and algorithms for non-destructive chlorophyll assessment in higher plant leaves. J. Plant Physiol. 160 (3), 271–282.

Gitelson, A.A., Keydan, G.P., Merzlyak, M.N., 2006. Three-band model for noninvasive estimation of chlorophyll, carotenoids, and anthocyanin contents in higher plant leaves. Geophys. Res. Lett. 33 (11).

Govaerts, Y.M., Verstraete, M.M., 1998. Raytran: a Monte Carlo ray-tracing model to compute light scattering in three-dimensional heterogeneous media. IEEE Trans. Geosci. Remote Sens. 36 (2), 493–505.

Houborg, R., Soegaard, H., Boegh, E., 2007. Combining vegetation index and model inversion methods for the extraction of key vegetation biophysical parameters using Terra and Aqua MODIS reflectance data. Remote Sens. Environ. 106 (1), 39–58.

Jacquemoud, S., Verhoef, W., Baret, F., Bacour, C., Zarco-Tejada, P.J., Asner, G.P., François, C., Ustin, S.L., 2009. PROSPECT+ SAIL models: a review of use for vegetation characterization. Remote Sens. Environ. 113, S56–S66.

Kuusk, A., 2001. A two-layer canopy reflectance model. J. Quant. Spectrosc. Radiat. Transf. 71 (1), 1–9.

Liu, S., Peng, Y., Du, W., Le, Y., Li, L., 2015. Remote estimation of leaf and canopy water content in winter wheat with different vertical distribution of water-related properties. Remote Sens. 7 (4), 4626–4650.

Martens, S.N., Ustin, S.L., Rousseau, R.A., 1993. Estimation of tree canopy leaf area index by gap fraction analysis. For. Ecol. Manag. 61 (1), 91–108.

Meroni, M., Rossini, M., Guanter, L., Alonso, L., Rascher, U., Colombo, R., Moreno, J., 2009. Remote sensing of solar-induced chlorophyll fluorescence: review of methods and applications. Remote Sens. Environ. 113 (10), 2037–2051.

Myneni, R.B., 1991. Modeling radiative transfer and photosynthesis in three-dimensional vegetation canopies. Agric. For. Meteorol. 55 (3-4), 323–344.

Nascimento, A.R.T., Fagg, J.M.F., Fagg, C.W., 2007. Canopy openness and LAI estimates in two seasonally deciduous forests on limestone outcrops in Central Brazil using hemispherical photographs. Revista Árvore 31 (1), 167–176.

Nocedal, J., Wright, S., 2006. Numerical optimization. Springer Science & Business Media.

Rascher, U., Alonso, L., Burkart, A., Cilia, C., Cogliati, S., Colombo, R., Damm, A., Drusch, M., Guanter, L., Hanus, J., et al., 2015. Sun-induced fluorescence-a new probe of photosynthesis: first maps from the imaging spectrometer HyPlant. Glob. Chang. Biol. 21 (12), 4673–4684.

Ustin, S.L., Gitelson, A.A., Jacquemoud, S., Schaepman, M., Asner, G.P., Gamon, J.A., Zarco-Tejada, P., 2009. Retrieval of foliar information about plant pigment systems from high resolution spectroscopy. Remote Sens. Environ. 113, S67–S77.

Valentinuz, O.R., Tollenaar, M., 2004. Vertical profile of leaf senescence during the grain-filling period in older and newer maize hybrids. Crop Sci. 44 (3), 827–834.

Van der Tol, C., Berry, J., Campbell, P., Rascher, U., 2014. Models of fluorescence and photosynthesis for interpreting measurements of solar-induced chlorophyll fluorescence. J. Geophys. Res. Biogeosci. 119 (12), 2312–2327.

Van der Tol, C., Rossini, M., Cogliati, S., Verhoef, W., Colombo, R., Rascher, U., Mohammed, G., 2016. A model and measurement comparison of diurnal cycles of sun-induced chlorophyll fluorescence of crops. Remote Sens. Environ. 186, 663–677.

Van der Tol, C., Verhoef, W., Timmermans, J., Verhoef, A., Su, Z., 2009. An integrated model of soil-canopy spectral radiances, photosynthesis, fluorescence, temperature and energy balance. Biogeosciences 6 (12), 3109–3129.

Verhoef, W., 1984. Light scattering by leaf layers with application to canopy reflectance modeling: the SAIL model. Remote Sens. Environ. 16 (2), 125–141.

Verhoef, W., 1985. Earth observation modeling based on layer scattering matrices. Remote Sens. Environ. 17 (2), 165–178.

Verhoef, W., 1998. Theory of Radiative Transfer Models Applied in Optical Remote Sensing of Vegetation Canopies. Wageningen University PhD Thesis.

Verhoef, W., Bach, H., 2007. Coupled soil-leaf-canopy and atmosphere radiative transfer modeling to simulate hyperspectral multi-angular surface reflectance and TOA radiance data. Remote Sens. Environ. 109 (2), 166–182.

Vilfan, N., van der Tol, C., Muller, O., Rascher, U., Verhoef, W., 2016. Fluspect-B: A model for leaf fluorescence, reflectance and transmittance spectra. Remote Sens. Environ. 186, 596–615.

Wang, Q., Li, P., 2013. Canopy vertical heterogeneity plays a critical role in reflectance simulation. Agric. For. Meteorol. 169, 111–121.

Widlowski, J.-L., Taberner, M., Pinty, B., Bruniquel-Pinel, V., Disney, M., Fernandes, R., Gastellu-Etchegorry, J.-P., Gobron, N., Kuusk, A., Lavergne, T., et al., 2007. Third Radiation Transfer Model Intercomparison (RAMI) exercise: documenting progress in canopy reflectance models. J. Geophys. Res.-Atmos. 112 (D9).

Zhang, Y., Guanter, L., Berry, J.A., Joiner, J., Tol, C., Huete, A., Gitelson, A., Voigt, M., Köhler, P., 2014. Estimation of vegetation photosynthetic capacity from space-based measurements of chlorophyll fluorescence for terrestrial biosphere models. Glob. Chang. Biol. 20 (12), 3727–3742.

Zhao, C., Li, H., Li, P., Yang, G., Gu, X., Lan, Y., 2017. Effect of vertical distribution of crop structure and biochemical parameters of winter wheat on canopy reflectance characteristics and spectral indices. IEEE Trans. Geosci. Remote Sens. 55 (1), 236–247.